



Micromechanical properties of TRISO coatings by in-situ high temperature nanoindentation and microcantilever fracture

Alex Leide^{a,b,*}, Eric Hintsala^c, Mark Davies^d, David T. Goddard^e, Dong Liu^b

^a UK Atomic Energy Authority, Culham Science Centre, Abingdon OX14 3DB, UK

^b School of Physics, University of Bristol, Tyndall Avenue, Bristol BS8 1TL, UK

^c Bruker Nano Surfaces & Metrology, 9625 West 76th St., Eden Prairie, MN 55434, USA

^d Ultra Safe Nuclear Corporation, St Helen's, UK

^e National Nuclear Laboratory, Preston Laboratory, Springfields, Preston PR4 0XJ, UK

ARTICLE INFO

Keywords:

TRISO
Nanoindentation
Micromechanics
Fracture
SiC

ABSTRACT

Coated nuclear fuel particles, most commonly tri-structural isotropic (TRISO), are intended for use in advanced high temperature reactors. It is vital to understand the mechanical properties of each coating layer to accurately predict the performance of these fuel particles and how these might change at each stage of their lifecycle. This paper reports results of in-situ nanoindentation, with an emphasis on the structural SiC layer, along with microcantilever testing of the critical SiC-IPyC interface. At 1000 °C the hardness of the SiC layer is ~75% lower than at room temperature implying significantly more plasticity at the reactor operating temperature. The elastic modulus was slightly lower at 1000 °C than at room temperature. Microcantilever fracture at the SiC-IPyC interface shows that failure occurs within the pyrolytic carbon layer rather than an interfacial “debonding” with a strength similar to that of bulk pyrolytic carbon.

1. Introduction

1.1. TRISO fuels and High Temperature Gas cooled Reactors

High temperature gas cooled reactors are favoured as a versatile advanced reactor which can efficiently generate electricity as well as high temperature process heat for industries such as hydrogen and chemical production. These reactors use coated particle fuels, typically with a TRISO (Tri-structural isotropic) coating structure [1,2]. These ~1 mm diameter spherical particles consist of a fissile kernel (~500 µm diameter) surrounded by a porous carbon “buffer” layer (~100 µm) and inner (IPyC) and outer (OPyC) pyrolytic carbon layers (~40 µm) sandwiching a β silicon carbide layer (~35 µm) [2]. The coatings are deposited onto fuel kernels using a fluidised bed chemical vapour deposition (FB-CVD) process which can mass-produce the millions of particles required to fuel a reactor. The particles are then embedded in a graphite or silicon carbide matrix to form pebbles or compacts to fuel pebble bed or prismatic reactors [3].

Extensive fuel performance models have been developed to predict the evolution of stresses and statistics of failure during the operating lifetime of TRISO fuels in various reactor scenarios, and to optimise the

structure of particle coatings [4–7]. Each material's temperature and irradiation-dependent properties used in fuel performance models are broadly derived from bulk material properties which have been gathered over many years [8]. Experimental verification of the material properties in the structure of microscopic fuel particles is challenging especially in the range of extreme environmental conditions which advanced high temperature reactors generate. Advanced methods to conduct these experiments have only recently been developed, therefore it will take some time to accumulate the required experimental data-points to populate and validate fuel performance models on the microscale.

1.2. Micromechanical testing of TRISO and SiC

Considering the small dimensions of the particles and their constituent layers, small-scale testing is required. Crush tests have been developed as a method for measuring the strength of particles [9–14], and have also been applied to hemispherical shells of silicon carbide which are extracted from particles [10,15]. Although crushing experiments measure the whole-particle strength, the experimental results are difficult to use in performance modelling, and the experimental

* Corresponding author at: UK Atomic Energy Authority, Culham Science Centre, Abingdon OX14 3DB, UK.

E-mail address: alex.leide@ukaea.uk (A. Leide).

<https://doi.org/10.1016/j.jeurceramsoc.2023.12.056>

Received 31 July 2023; Received in revised form 12 December 2023; Accepted 13 December 2023

Available online 15 December 2023

0955-2219/Crown Copyright © 2023 Published by Elsevier Ltd. This is an open access article under the CC BY license (<http://creativecommons.org/licenses/by/4.0/>).

conditions do not replicate those found during operation. Nanoindentation has been performed on various grades of TRISO coating layer, both at room temperature [15–19], and at elevated temperatures [18,19] to obtain the hardness and modulus of the constituent materials. At room temperature, the CVD SiC layer of TRISO particles has a lower elastic modulus and hardness than bulk CVD SiC [17,19], but a smaller temperature-dependent change up to 500 °C [19]. Similar results were observed for nanoindentation up to 500 °C on SiC_f/SiC composites, including on neutron irradiated specimens [20]. These results showed minimal influence of microstructure as SiC_f/SiC typically has a columnar microstructure in the matrix whereas TRISO particle coatings are equiaxed; porosity, chemical composition, and residual stresses may have larger effects.

Microcantilever bending was conducted by Zhao *et al.* on the SiC layer of a coated particle to investigate the fracture toughness in radial and circumferential directions, finding anisotropic properties at room temperature with a higher fracture toughness ($6.72 \text{ MPa}\cdot\text{m}^{0.5}$) for crack propagation in the radial direction than the tangential (hoop) direction ($3.47 \text{ MPa}\cdot\text{m}^{0.5}$), related to intergranular fracture between the columnar grains [21]. It is desirable for SiC in coated fuel particles to have an equiaxed grain structure to minimise radial diffusion pathways for transmutation products and to have isotropic thermomechanical properties. Similar results for fracture toughness were observed in microcantilever tests in [15] which gave fracture toughness between 3.79 and $7.99 \text{ MPa}\cdot\text{m}^{0.5}$ depending on specimen manufacturing conditions. In the same paper, nanoindentation fracture was used to determine fracture toughness, finding an apparently higher toughness in the radial direction; however, indentation fracture toughness should not be used for material property evaluation when cracks are not equal lengths, nor when non-equibiaxial residual stresses may be present as in this case. Cracks from the indenter corners close to the circumferential direction followed the curvature of the SiC coating and were longer than cracks in the radial direction suggesting a complex stress state [15]. Zayachuk *et al.* performed microcantilever fracture toughness tests in SiC_f/SiC composites including the columnar SiC matrix finding no systematic difference in toughness for cantilevers at different orientations, being $\sim 4.25 \text{ MPa}\cdot\text{m}^{0.5}$ which is intermediate between the radial and circumferential direction fracture toughness of TRISO particles [22]. Residual stresses in SiC_f/SiC composites are unlikely to be as significant as those in spherical coated particles, suggesting that the apparent differences in fracture toughness in TRISO particles are caused by stress state.

2. Materials and methods

2.1. Samples

Specimens of prototype fully ceramic microencapsulated (FCM) fuel pellets were provided by Ultra Safe Nuclear Corporation (USNC), and contained surrogate TRISO particles embedded in a silicon carbide matrix. This particular prototype pellet was made using a process similar to reported in reference [23]. The surrogate particles in the pellet are manufactured by fluidised bed chemical vapour deposition over zirconia kernels with a coating structure based on the US HTGR designs developed in the AGR development programmes. Different manufacturing conditions and their effects on properties are reviewed in references [1, 24]. The pellet was sectioned using a low-speed diamond saw followed by mechanical grinding and polishing to a 1 µm diamond finish. The silicon carbide matrix provides a stiff mounting for the TRISO particles which remains stable to high temperatures. A schematic of the sectioned and polished FCM is shown in Fig. 1 with a side view and top-down view of the cross section. The position of particles in the SiC matrix determines which section of the particle cross-section is revealed on the polished surface: the largest diameter cross-section particles are closest to their equatorial plane and are chosen for analysis. An SEM image of the specimen mounted in the Bruker PI-89 in-SEM PicoIndenter is shown in Supplementary Material showing the benefit of the larger specimen

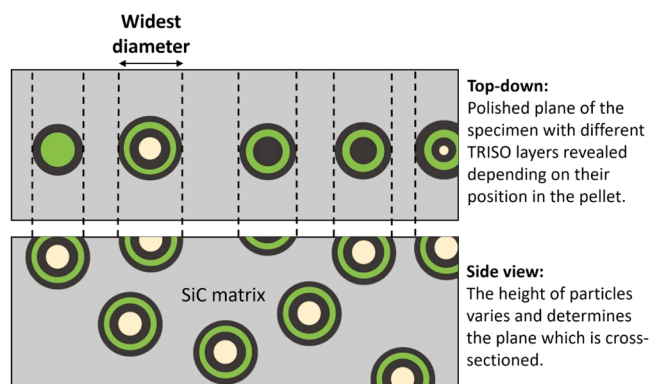


Fig. 1. Schematic of FCM sample preparation with embedded TRISO surrogate particles. Different height particles in the side view of the specimen reveal different cross-sections in the polished surface.

for clamping into position.

2.2. Nanoindentation

In situ indentation was carried out using a Bruker PI-89 PicoIndenter with a polycrystalline cubic boron nitride Berkovich tip inside a Thermo Fisher Versa3D dualbeam FIB/SEM. The area function of the tip was calibrated using a standard fused silica sample before and after the tests and inspected using the SEM to investigate tip wear following high temperature indentation. The indenter was operated in load controlled continuous measurement of X (CMX) mode at 50 Hz to obtain properties as a function of depth up to a peak force of 150 or 300 mN over a 60 s linear loading. Measurements were made on the SiC layer at room temperature and 1000 °C. Prior to gathering the high temperature indentation data, temperature matching of the tip and sample was confirmed by holding the tip and sample in contact at 50 mN and monitoring for any temperature flow between the two bodies. Vacuum levels inside the chamber were 8×10^{-4} Pa at room temperature and rose slightly to 9×10^{-4} Pa at 1000 °C, within the operating limit of the microscope at $\sim 2 \times 10^{-3}$ Pa.

Ex situ indentation was carried out using a Hysitron TI Premier (Bruker, USA) nanoindenter to investigate fracture around indentations as a function of position in the SiC layer. Quasi-static load-controlled indentations were made following the ISO 14577 recommendations [25], and indentation impressions were imaged using optical microscopy and SEM.

2.3. Microcantilever preparation and testing

Six microcantilevers were made at the SiC/PyC interfaces of TRISO particles with the base in the SiC and the beam extending into the pyrolytic carbon. The cantilevers were prepared using focussed ion beam milling in a FEI Nanolab 600 dualbeam FIB/SEM using 30 kV gallium ions. Coarse milling was carried out with a beam current of 6.5 nA and polishing using 0.46 nA to create a nominally right-angle triangular cross-section cantilever. Actual dimensions were measured using the SEM, accounting for tilt correction when measuring the cantilever height.

Three cantilever beam tests of the IPyC/SiC interface were conducted ex-situ at room temperature using a Hysitron TI Premier (Bruker, USA) nanoindenter with a diamond Berkovich tip. The cantilevers were imaged using the nanoindenter in scanning probe mode to identify the loading location, then load was applied using displacement control at 5 nm/s until failure. Stress at the fracture point and maximum strain were calculated from the cantilever dimensions and the distance of the loading point based on simple beam theory, as described in [26]. Un-notched cantilevers were used in this work to investigate the failure

strength of the boundary as opposed to the fracture toughness which is derived using notched cantilevers. Cantilevers were imaged using the FEI Nanolab SEM post-testing to observe the fracture mechanisms. Three remaining cantilevers were sent for 1000 °C in-situ testing using the same Bruker PI-89 high temperature micromechanical test system in a Thermo Fisher Versa 3D FIB/SEM; however, on heating above 800 °C in the microscope vacuum significant oxidation occurred resulting in the loss of the microcantilevers. The observed oxidation will be discussed later.

2.4. Cross-section characterisation

Following high temperature micromechanical testing, cross sections were milled at the interfaces to observe the sub-surface interfacial structure and the depth of oxidation. An initial large cross-section trench was milled using a Tescan Amber X xenon P-FIB with local polishing cross-sections using a FEI Helios Ga-FIB.

3. Results

3.1. In-situ nanoindentation

CMX load displacement curves are shown in Fig. 2. At room temperature the curves follow the expected shape for a brittle material showing mostly elastic deformation with small pop-in events during loading. At 1000 °C, the loading segment of the curves is almost straight indicating more plastic deformation during loading, which is also identified by the larger residual indentation depth after unloading. An apparent pop-in event occurs at ~60 nm displacement for both room temperature and high temperature indentations; load-displacement graphs highlighting this are shown in [supplementary material](#). At depths lower than 60 nm, there is no dynamic oscillation as this can cause damage to the sample; the dynamic segment begins at 60 nm which may cause the apparent pop-in event here. Fracture occurs on unloading the indenter, and is not represented in the load-displacement curves.

At room temperature, SiC has a hardness of 38.8 ± 0.45 GPa and Young's modulus of 467 ± 6.75 GPa averaged across the two indents at depths greater than 100 nm. This is in line with the accepted properties for room temperature SiC, and remains constant with indentation depth. The near-surface properties below 100 nm contact depth are dominated by tip area function variability and contact mechanics, and are less reliable for quantification. To derive Young's modulus from the reduced modulus output from nanoindentation, the Young's modulus of cBN was assumed to be 672 GPa, and Poisson ratio of 0.19 based on measurements made by Bruker during development of these indenter tips. Reduced modulus is plotted in Fig. 3 for comparison with the high temperature indentation where the temperature dependent mechanical

properties of the cBN tip are not fully understood.

For 1000 °C nanoindentation, the measured hardness is much lower than at room temperature, being between 11 GPa and dropping to 8 GPa with increasing depth. The reduced modulus is less affected by increasing temperature being ~260 GPa at 200 nm; however, this decreases with contact depth to ~240 GPa at 900 nm. The average hardness at 1000 °C is 9.13 ± 0.85 GPa and average Young's modulus is 347 ± 21.7 GPa, as plotted on Fig. 4.

The results of this work continue the linear trend of reduction in hardness and elastic modulus with increasing test temperature which is found up to 500 °C in the literature and plotted in Fig. 4 [19,20]. While the reduction in hardness is significant, the reduction in elastic modulus is comparatively minor. The larger error bars for elastic properties are likely to be caused by the longer-range environment which contributes to indentation elastic properties; a larger spatial volume contributes to elastic properties, therefore in TRISO SiC the neighbouring pyrolytic carbon layers may be influencing the measured properties. At 1000 °C the loss of material by oxidation may further be reducing the measured elastic modulus as a function of depth for larger indentations.

Following indentation at 1000 °C, the area function of the cBN tip was re-calibrated, finding minimal difference between the calibration prior to 1000 °C testing (Fig. 5). The tip was also imaged by SEM, showing that it has maintained its shape despite the large number of indentations made in hard silicon carbide during calibrations and method development. The contrast on the tip may be a surface oxide or material transfer onto the tip, however this has not affected the area function at the depths of interest.

3.2. Indentation deformation

Room temperature indentations show crack patterns which vary as a function of position in the SiC layer (Fig. 6(a) and (b)). Closer to the centreline of the coating layer, cracks emanate from the corners of indentations as expected, with cracks in the particle circumferential direction being longer. Closer to the IPyC interface, crack lengths are considerably larger, possibly due to less structural confinement by the nearby pyrolytic carbon layer reducing the compressive stresses around indents. Cracks in the particle radial direction remain short. Fig. 6(c) shows the impression of an indentation made at 1000 °C, with slip lines clearly visible from the lower right corner of the indentation, and minimal fracture.

3.3. Interfacial microcantilever fracture

Stress-strain curves are shown in Fig. 7 for the three microcantilevers made at the SiC-IPyC interface and tested at room temperature. Cantilever 2 is anomalous in not showing a large load drop corresponding to brittle failure and rapid crack propagation as seen in Cantilever 1 and 3.

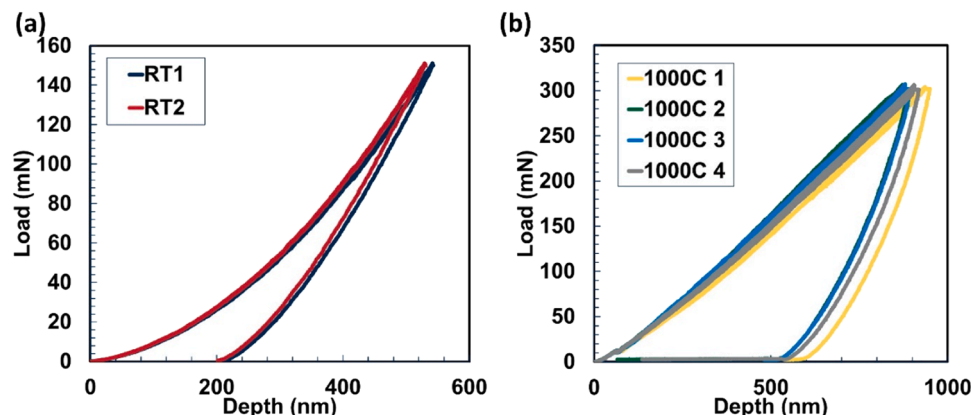


Fig. 2. Load-displacement curves for in-situ indentation at (a) room temperature, and (b) 1000 °C.

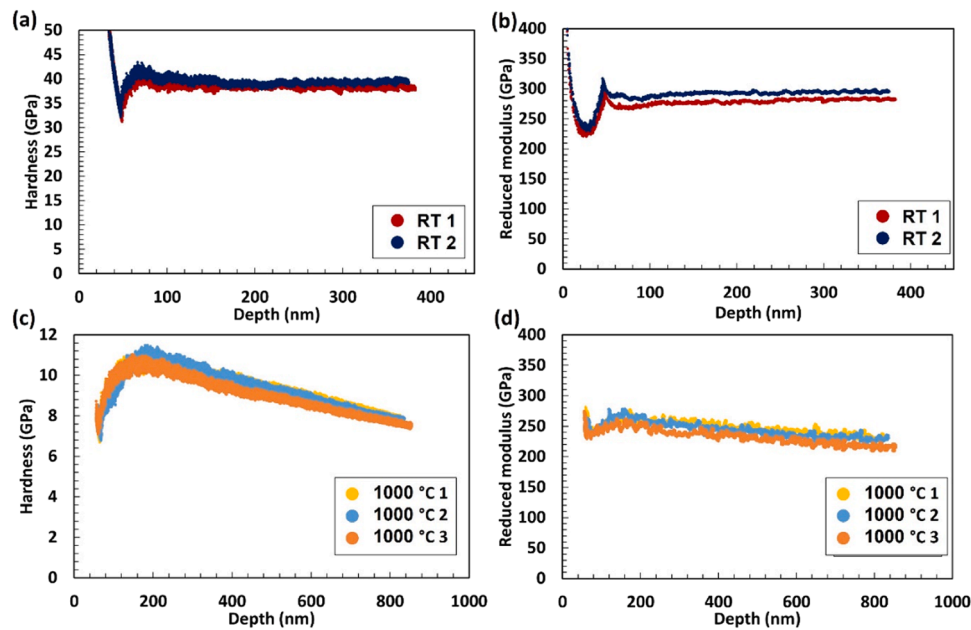


Fig. 3. Hardness and reduced modulus as a function of depth for indentations in TRISO SiC at room temperature (a) and (b), and 1000 °C (c) and (d).

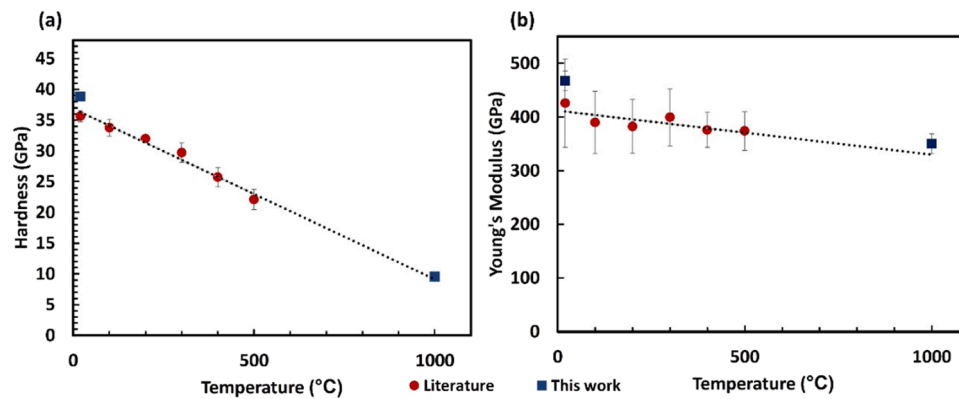


Fig. 4. Comparison of high temperature nanoindentation literature data from [19,20] and this work. (a) hardness, and (b) Young's modulus.

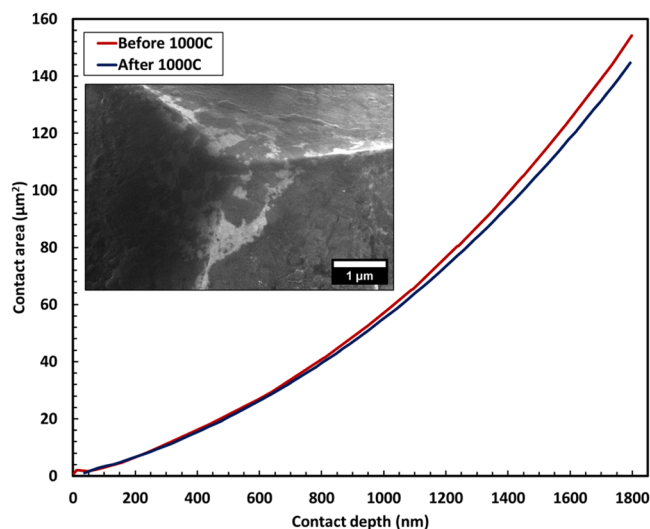


Fig. 5. Comparison of tip area functions before and after 1000 °C indentations with SEM image of indenter tip after all 1000 °C indentations.

This cantilever was unloaded prior to complete failure. Cantilever 1 shows several load-drop events in the displacement-controlled test indicating microfracture events prior to complete failure, whereas Cantilever 3 shows sudden brittle failure.

In all three cases the cantilever beam remained attached to the base after the bending experiment (Fig. 8). This may be due to ligaments remaining attached between the interfaces. Cantilever 1 which shows small load drops during measurement has a crack path through PyC which is being deflected at the locations of SiC at this interface. These deflections appear to give some limited toughening. Cantilever 3 which gives linear loading and sharp brittle failure shows a straight crack with no deflections visible on the surface. Cantilever 2 was anomalous in the loading experiment with a low initial failure stress followed by a high strain prior to unloading the indenter. The crack path appears to follow pores, and is deflected significantly rather than following the straight path as in Cantilever 3.

Milling through the TRISO particle using a P-FIB rapidly exposed the cross-section of the particle coating layers, however redeposited material obscured the view of the interfaces. Polishing local regions using a Ga-FIB gave higher quality surfaces for revealing the microstructure of the interfaces between SiC and pyrolytic carbon layers. Fig. 9 shows the significant differences between the interfaces between SiC and IPyC or OPyC. The SiC/IPyC interface is interlocked as SiC has partially

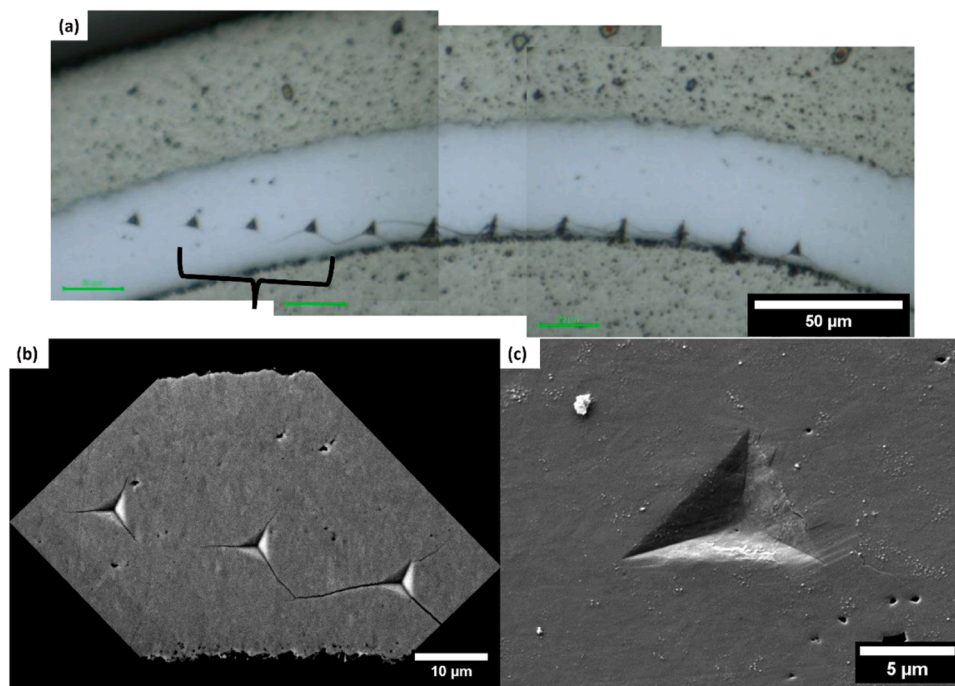


Fig. 6. (a) Montage of optical micrographs of a linescan of nanoindentations in the SiC layer of a TRISO particle. Indentation cracks are short in the radial direction of the particle. (b) SEM magnified view of the three indentations indicated in (a). (c) indentation impression made at 1000 °C showing signs of plastic deformation near the indent corners.

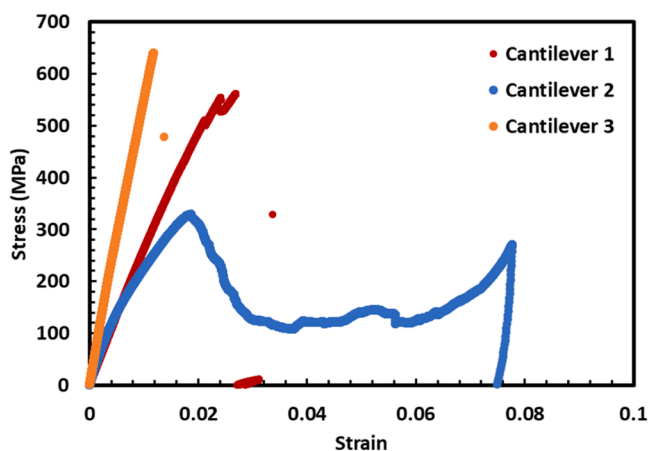


Fig. 7. Maximum bending stress-strain curves calculated from microcantilever dimensions and load-displacement data acquired during the experiment.

deposited into pyrolytic carbon pores, while larger pores remain than in the bulk of the IPyC. The SiC/IPyC interlocking region is $\sim 1.2 \mu\text{m}$ wide and the high porosity region extends $\sim 2.8 \mu\text{m}$ from the SiC interface, indicated in Fig. 9. In contrast, the SiC/OPyC interface is smooth with no variation in OPyC density between the bulk and the interface. A full pore analysis by 3D FIB sectioning and image segmentation is out of the scope of this work, but has been conducted recently on other particles [27,28]. The surface morphology seen in Fig. 9(a), and the surface height change in (b) and (c) are related to the high temperature oxidation which occurred during the 1000 °C indentations. The height loss appears to be the same in IPyC and OPyC. Further images are shown in [supplementary material](#).

4. Discussion

4.1. High temperature micromechanical properties

High temperature mechanical properties of SiC are significantly different to room temperature properties, and therefore need to be considered in the design of reactors and components. Most significant is the reduction in hardness and the appearance of plastic deformation around indentations at 1000 °C. Enhanced plasticity at the reactor operating temperature will improve safety margins in the fuel reducing the likelihood of a brittle failure during operation, allowing longer operation and improved burnup.

The primary slip system in 3C-SiC is $\langle 110 \rangle \{111\}$ and may correspond to the “pop-in” event at $\sim 60 \text{ nm}$ which is consistently observed around this depth in the literature and in this work [29,30]. This depth also corresponds to the activation of the dynamic oscillation segment for depth sensing measurement, which may be impacting the onset of plasticity, potentially causing this pop-in event to occur. Both references [29,30] also use dynamic continuous stiffness nanoindentation, although it is not clear in their work if the onset of this segment was delayed to 60 nm as was done during the indentations here. The exact onset of plasticity will vary depending on the orientation of the grain being indented and the resolved shear stress; Zhao *et al.* also found the pop-in occurring between 55 – 70 nm displacement and 8 – 9 mN load [29]. Molecular dynamics simulations of very low displacement ($< 7 \text{ nm}$) indentation in SiC shows that prior to the complete dislocation slip, partial dislocations of type $\frac{1}{6}[\bar{1}2\bar{1}] + \frac{1}{6}[\bar{2}11] = \frac{1}{2}[\bar{1}10]$ form to allow slip with a stacking fault between [31]. Additionally, strain rate can affect the onset of plasticity, as discussed in [32,33], with lower strain rates inducing plasticity in 4H-SiC at lower loads. This is explained by a thermally activated defect nucleation mechanism where slower indentations have more chance of nucleating dislocations in finite time during the test; the thermal activation of plasticity increases with increasing temperature.

With the limited slip systems, dislocation mobility is low at room temperature, leading to a large proportion of elastic deformation in the

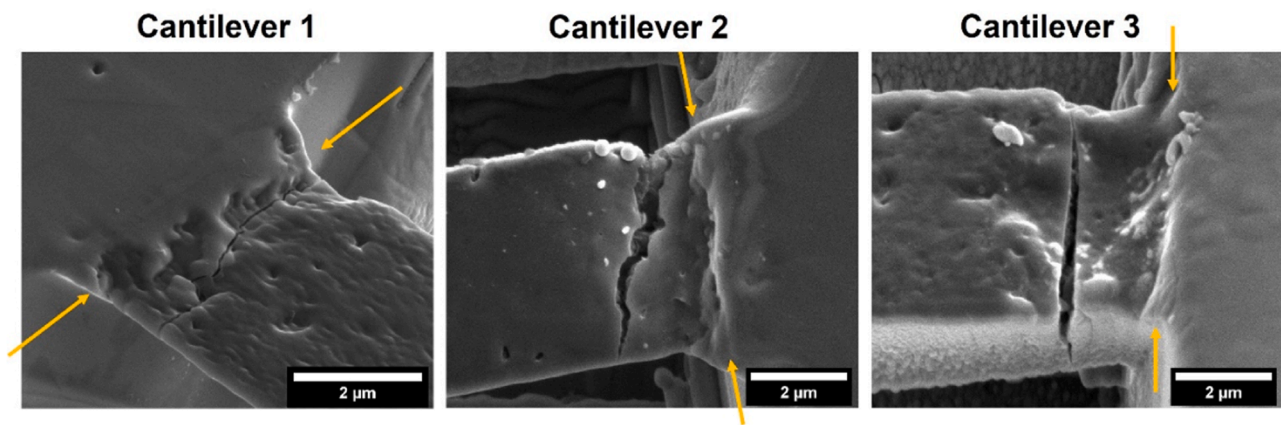


Fig. 8. SEM images of fractured cantilevers. Arrows indicate location of IPyC/SiC interface.

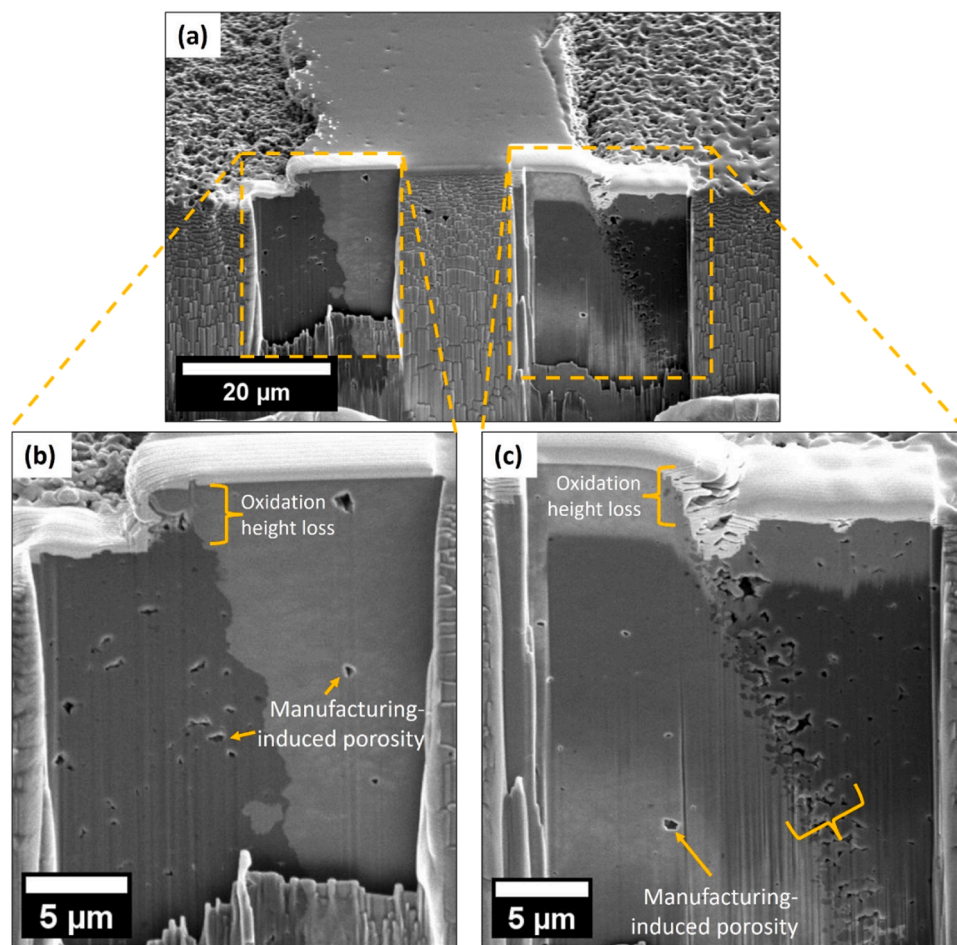


Fig. 9. (a) P-FIB cross-section of a TRISO particle with zoomed regions polished by Ga-FIB showing the interfaces of (b) OpyC-SiC and (c) IPyC-SiC. The surface height loss and porosity are indicated, including the interlocking and residual porosity at the SiC-IPyC interface.

elastic-plastic loading regime, followed by fracture during unloading to accommodate the deformation. Thermal activation of cross-slip in SiC has been reported, in particular for α -SiC which has been more widely studied [32]. In those cases, thermally activated cross-slip occurs via dislocation dissociation into partials, similar to the case in 3C-SiC at room temperature. At the 1000 °C indentation temperature in this work, thermally activated slip has enhanced plastic deformation and reduced fracture around indentations.

Previous high temperature indentation of SiC layers in TRISO

particles found a linear reduction in elastic modulus up to 500 °C with a trend of $E = E_0 - 0.07 T$ where E_0 is the room temperature elastic modulus, and T is temperature in degrees Celsius [18]. The results in this work match this trend, where $E_0 = 467$ GPa, and $E = \sim 350$ GPa at 1000 °C at 200 nm depth. At 1000 °C, the fuel performance modelling handbook suggests at 5% reduction in elastic modulus with 4% uncertainty based on macroscopic methods, a far smaller reduction than measured using nanoindentation here, and based on the experimental trend [8]. This may be related to the lengthscale of nucleating thermally

activated defects. The reduction in elastic modulus is related to interatomic bond strength which reduces with increasing thermal energy. The elastic modulus of different grades of SiC responded differently to high temperature indentation; those with larger grain size had a stronger temperature dependence [19]. Nevertheless, the reduction in elastic modulus with temperature is relatively small and remains approximately ten times larger than the neighbouring pyrolytic carbon layers so will have a minimal effect on fuel performance and stress evolution during operation.

4.2. Interfacial properties

The interlocked and porous SiC/IPyC interfacial structures is in agreement with recent work which showed that fission products can be trapped in the pores near the IPyC/SiC interface [27]. The interlocking of SiC into IPyC and remaining local porosity may act as stress concentrators during irradiation-induced dimensional changes leading to premature failure of the IPyC compared to a smooth interface where strains are accommodated over a larger area. The accumulation of fission products at this interface may further influence the stress concentration effects at pores, for example by forming precipitates or causing local corrosion [34]. The significant difference between SiC/IPyC and SiC/OPyC implies their properties will be quite different both mechanically and functionally in terms of fission product retention, thermal transport, and corrosion.

Fractured microcantilevers at the SiC/IPyC interface showed that fracture occurred in the pyrolytic carbon rather than as a debonding of the interface. This somewhat simplifies the evaluation of interfacial strength in coated particles as the interface can be assumed strongly bonded, while the circumferential failure can be considered as a failure of the pyrolytic carbon itself. This is in agreement with recent observations in finite element simulations of particle interactions in [35]. Bokros studied the strength of various forms of pyrolytic carbon, finding a flexural strength of ~ 550 MPa for dense isotropic carbon deposited from gases [36]. The structure of pyrolytic carbons in that work is similar to the pyrolytic carbon layers in TRISO particles, and the strength is close to the measured values in this work. Additionally, X-ray tomography of coated particles post-irradiation shows segments of the pyrolytic carbon buffer remaining attached to the SiC layer and the shrinkage crack propagating through the carbon itself rather than by debonding at the interface, and also segments of buffer remaining attached to the SiC layer during crushing experiments [9].

After the cantilever fracture experiments, the cantilevers rebounded and the cantilever beam was not fully detached. This crack closure has also been observed in microcantilever fracture in graphite; an explanation based on bridging across the tortuous fracture surface, and elastic recovery of the material ahead of the crack appears to also apply here [37]. On the microscale, fracture appears more “graceful” in carbon as the distribution of pores reduces the likelihood of catastrophic failure in the small volumes being tested, compared to macroscale mechanical testing of porous carbons. This may explain the higher strengths found here than in the literature for pyrolytic carbon; nevertheless, these microcantilever tests are on the representative lengthscale of coated fuel particles.

4.3. In-situ high temperature indentation testing

High temperature indentation requires a temperature resilient indenter material. In this work, cubic boron nitride (cBN) was used as it maintains hardness and shape in a high temperature oxidising environment better than diamond, therefore giving more reliable tip area functions across multiple indentation tests, and a longer tip lifetime. For indenting soft and compliant materials such as metals, cBN is more than sufficient in hardness and elastic modulus; however, as the hardness of the tip is close to the SiC material in the specimen some deformation may occur in the tip during the test, making the SiC appear harder. This

may explain the slightly higher room temperature hardness measured in this work than in comparable literature where diamond nanoindenter tips have been used [19,20]. Additionally, cBN has a different Poisson ratio to diamond, requiring a different conversion from reduced modulus to Young’s modulus which may also change the derived values, however, those presented here are closer to those measured in bulk CVD SiC than the relatively low values for Young’s modulus typically reported for TRISO particles [19]. Specimen mounting for indentation is also critical as compliant materials can give apparently lower elastic modulus measurements. In references [18,19] individual TRISO particles were mounted in high temperature cement which may introduce compliance to the system. The particles in this work are mounted in a dense silicon carbide matrix which is stiffer than other high temperature mounting media giving more reliable results. The FCM SiC material containing TRISO particles was polished with parallel faces to ensure a good mechanical mounting to the clip holder on the indenter, making handling easier and the temperature more stable in the high conductivity SiC compared to typical high temperature cements.

The oxidation of pyrolytic carbon which occurred during high temperature experiments prevented high temperature microcantilever bend testing as these were lost. During heating, the cantilevers were intact up to 800°C , and the surface of the pyrolytic carbon was as-polished during a 2 h hold at this temperature. The ~ 1 h heating step from $800 - 1000^\circ\text{C}$ resulted in oxidation and $\sim 2\ \mu\text{m}$ surface loss, which did not increase during subsequent high temperature experiments. This temperature approximately corresponds to the transition from so-called Regime 2 to Regime 3 oxidation described in references [38,39]. Regimes 1 and 2 are kinetically rate limited, so do not detectably occur in the low oxygen environment of a SEM chamber; however, in Regime 3 termed “boundary-layer controlled” the kinetic reaction rate is sufficiently high to be limited by oxygen supply. Considering the rapid initial oxidation, then no further evolution, the oxidation may be caused by oxygen molecules adhered to the specimen or chamber surface which are then consumed by an initial fast oxidation. The oxidised structure of pyrolytic carbons is highly porous on the surface, shown in Fig. 9 and supplementary material, and is comparable to the microstructures of oxidised matrix graphite in [40]. Lower magnification imaging reveals circumferential texture in the buffer and PyC layers which is presumably caused by the deposition conditions and as manufactured structure of the particles (see supplementary material). Additionally, oxidised surfaces in IPyC and OPyC appear different, and may be traced back to manufacturing differences which also result in differences in other properties. The FIB cross-sections in Fig. 9 show that the oxidation-induced porosity is confined to the near-surface of the particle, further implying that the carbon oxidation was in Regime 3.

5. Conclusions

High temperature nanoindentation at the operating temperature of HTGRs reveals significantly temperature dependant mechanical properties in the SiC layer of TRISO particles. The enhanced plastic deformation is beneficial to the integrity of these fuels during operation, reducing the chances of brittle failure and improving the potential performance of the fuel.

Interfaces between SiC and PyC layers in TRISO particles are of interest for the “debonding” failure mechanisms. Microcantilever bending tests showed that the direct SiC/PyC interface is strong, leading to fracture occurring within the PyC layer itself rather than by a debonding mechanism. This implies that “bulk” properties of the PyC materials can be used for mechanical modelling with a “strong” interface rather than needing to explicitly account for interfacial strength. The microstructure of the inner and outer SiC/PyC interfaces is different, possibly leading to significant differences in their functional performance.

The SiC layer in TRISO particles shows anisotropic fracture properties, whereby indentation cracks are longer in the tangential direction than the radial direction of the polished cross-sectioned particle. This

crack pattern is not affected by the microstructure suggesting it is a result of residual stresses in the TRISO coating with a tensile residual stress in the radial direction (opening tangential cracks), and compression in the hoop direction (opposing radial cracks. This is beneficial for integrity of TRISO particles, however, must be considered in modelling efforts.

CRedit authorship contribution statement

Alex Leide: Conceptualisation, Methodology, Formal analysis, Investigation, Writing – original draft, Visualisation, Project administration. **Eric Hinstanta:** Methodology, Formal analysis, Investigation, Resources, Writing – review & editing, Project administration. **Mark Davies:** Resources, Supervision, Funding acquisition. **David T. Goddard:** Resources, Supervision, Funding acquisition. **Dong Liu:** Conceptualisation, Resources, Writing – review & editing, Supervision, Project administration, Funding acquisition.

Declaration of Competing Interest

The authors declare that they have no known competing financial interests or personal relationships that could have appeared to influence the work reported in this paper.

Acknowledgements

This research was funded under the £46 m Advanced Fuel Cycle Programme as part of the Department for Business, Energy, and Industrial Strategy's (BEIS) £ 505 m Energy Innovation Programme. This project was supported by the Royal Academy of Engineering under the Research Fellowship programme. The research used UKAEA's Materials Research Facility, which has been funded by and is part of the UK's National Nuclear User Facility and Henry Royce Institute for Advanced Materials. The authors thank Dr Ed Eardley for operation of the Tescan Amber X P-FIB.

Appendix A. Supporting information

Supplementary data associated with this article can be found in the online version at [doi:10.1016/j.jeurceramsoc.2023.12.056](https://doi.org/10.1016/j.jeurceramsoc.2023.12.056).

References

- [1] P.A. Demkowicz, B. Liu, J.D. Hunn, Coated particle fuel: historical perspectives and current progress, *J. Nucl. Mater.* 515 (2019) 434–450, <https://doi.org/10.1016/j.jnucmat.2018.09.044>.
- [2] K. Verfondern, H. Nabelek, J.M. Kendall, Coated particle fuel for high temperature gas cooled reactors, *Nucl. Eng. Technol.* 39 (2007) 603–616, <https://doi.org/10.5516/net.2007.39.5.603>.
- [3] C. Lu, B.D. Hiscox, K.A. Terrani, N.R. Brown, Fully ceramic microencapsulated fuel in prismatic high temperature gas-cooled reactors: analysis of reactor performance and safety characteristics, *Ann. Nucl. Energy* 114 (2018) 277–287, <https://doi.org/10.1016/j.anucene.2017.12.021>.
- [4] J.J. Powers, B.D. Wirth, A review of TRISO fuel performance models, *J. Nucl. Mater.* 405 (2010) 74–82, <https://doi.org/10.1016/j.jnucmat.2010.07.030>.
- [5] W.F. Skerjanc, J.T. Maki, B.P. Collin, D.A. Petti, Evaluation of design parameters for TRISO-coated fuel particles to establish manufacturing critical limits using PARFUME, *J. Nucl. Mater.* 469 (2016) 99–105, <https://doi.org/10.1016/j.jnucmat.2015.11.027>.
- [6] R. Li, B. Liu, C. Tang, Sensitivity of stresses in TRISO-coated fuel particles to the coating layer properties, *Nucl. Eng. Des.* 307 (2016) 309–318, <https://doi.org/10.1016/j.nucengdes.2016.07.010>.
- [7] M.A. Stawicki, Benchmarking of the MIT High Temperature Gas-Cooled Reactor TRISO-Coated Particle Fuel Performance Model, Massachusetts Institute of Technology, 2006.
- [8] L.L. Snead, T. Nozawa, Y. Katoh, T.-S. Byun, S. Kondo, D.A. Petti, Handbook of SiC properties for fuel performance modeling, *J. Nucl. Mater.* 371 (2007) 329–377, <https://doi.org/10.1016/j.jnucmat.2007.05.016>.
- [9] D. Liu, S. Knol, J. Ell, H. Barnard, M. Davies, J.A. Vreeling, R.O. Ritchie, X-ray tomography study on the crushing strength and irradiation behaviour of dedicated tristructural isotropic nuclear fuel particles at 1000 °C, *Mater. Des.* 187 (2020), 108382, <https://doi.org/10.1016/j.matdes.2019.108382>.
- [10] T.S. Byun, J.D. Hunn, J.H. Miller, L.L. Snead, J.W. Kim, Evaluation of fracture stress for the SiC layer of TRISO-coated fuel particles using a modified crush test method, *Int. J. Appl. Ceram. Technol.* 7 (2010) 327–337, <https://doi.org/10.1111/j.1744-7402.2009.02462.x>.
- [11] A. Briggs, R.W. Davidge, C. Padgett, S. Quickenden, Crushing behaviour of high temperature reactor coated fuel particles, *J. Nucl. Mater.* 61 (1976) 233–242, [https://doi.org/10.1016/0022-3115\(76\)90262-2](https://doi.org/10.1016/0022-3115(76)90262-2).
- [12] T. Ogawa, K. Ikawa, Crushing strengths of SiC-Triso and ZrC-Triso coated fuel particles, *J. Nucl. Mater.* 98 (1981) 18–26, [https://doi.org/10.1016/0022-3115\(81\)90383-4](https://doi.org/10.1016/0022-3115(81)90383-4).
- [13] R.D. Cromarty, G.T. Van Rooyen, J.P.R. De Villiers, Crush strength of silicon carbide coated TRISO particles: influence of test method and process variables, *J. Nucl. Mater.* 445 (2014) 30–36, <https://doi.org/10.1016/j.jnucmat.2013.10.041>.
- [14] K. Minato, K. Fukuda, K. Ikawa, H. Matsushima, S. Kurobane, Crushing strength of irradiated Triso coated fuel particles, *J. Nucl. Mater.* 119 (1983) 326–332, [https://doi.org/10.1016/0022-3115\(83\)90211-8](https://doi.org/10.1016/0022-3115(83)90211-8).
- [15] P. Hosemann, J.N. Martos, D. Frazer, G. Vasudevamurthy, T.S. Byun, J.D. Hunn, B. C. Jolly, K. Terrani, M. Okuniewski, Mechanical characteristics of SiC coating layer in TRISO fuel particles, *J. Nucl. Mater.* 442 (2013) 133–142, <https://doi.org/10.1016/j.jnucmat.2013.08.041>.
- [16] R.L. Seibert, B.C. Jolly, M. Baloch, D.P. Schappel, K.A. Terrani, Production and characterization of TRISO fuel particles with multilayered SiC, *J. Nucl. Mater.* 515 (2019) 215–226, <https://doi.org/10.1016/j.jnucmat.2018.12.024>.
- [17] J. Tan, P.J. Meadows, D. Zhang, X. Chen, E. López-Honorato, X. Zhao, F. Yang, T. Abram, P. Xiao, Young's modulus measurements of SiC coatings on spherical particles by using nanoindentation, *J. Nucl. Mater.* 393 (2009) 22–29, <https://doi.org/10.1016/j.jnucmat.2009.05.001>.
- [18] N. Rohbeck, D. Tsioulas, I.P. Shapiro, P. Xiao, S. Knol, J.M. Esclaine, M. Perez, In situ nanoindentation of irradiated silicon carbide in TRISO particle fuel up to 500 °C, *J. Nucl. Mater.* 465 (2015) 692–694, <https://doi.org/10.1016/j.jnucmat.2015.06.035>.
- [19] N. Rohbeck, D. Tsioulas, I.P. Shapiro, P. Xiao, S. Knol, J.M. Esclaine, M. Perez, B. Liu, Comparison study of silicon carbide coatings produced at different deposition conditions with use of high temperature nanoindentation, *J. Mater. Sci.* 52 (2017) 1868–1882, <https://doi.org/10.1007/s10853-016-0476-5>.
- [20] D. Frazer, C.P. Deck, P. Hosemann, High-Temperature Nanoindentation of SiC/SiC Composites, *Jom* 72 (2020) 139–144, <https://doi.org/10.1007/s11837-019-03860-7>.
- [21] X. Zhao, R.M. Langford, J. Tan, P. Xiao, Mechanical properties of SiC coatings on spherical particles measured using the micro-beam method, *Scr. Mater.* 59 (2008) 39–42, <https://doi.org/10.1016/j.scriptamat.2008.02.022>.
- [22] Y. Zayachuk, P. Karamched, C. Deck, P. Hosemann, D.E.J. Armstrong, Linking microstructure and local mechanical properties in SiC-SiC fiber composite using micromechanical testing, *Acta Mater.* 168 (2019) 178–189, <https://doi.org/10.1016/j.actamat.2019.02.001>.
- [23] C. Ang, L. Snead, Y. Kato, A logical approach for zero-rupture Fully Ceramic Microencapsulated (FCM) fuels via pressure-assisted sintering route, *J. Nucl. Mater.* 531 (2020), 151987, <https://doi.org/10.1016/j.jnucmat.2020.151987>.
- [24] A. Battistini, T.A. Haynes, D. Shepherd, M.R. Wenman, Residual stresses in as-manufactured TRISO Coated Particle Fuel (CPF), *J. Nucl. Mater.* 586 (2023), 154659, <https://doi.org/10.1016/j.jnucmat.2023.154659>.
- [25] "Metallic Materials – Instrumented indentation test for hardness and materials parameters," ISO 14577, (2015). (<https://www.iso.org/obp/ui/#iso:std:iso:14577:1:ed-2:vi:en>).
- [26] D. Di Maio, S.G. Roberts, Measuring fracture toughness of coatings using focused-ion-beam-machined microbeams, *J. Mater. Res.* 20 (2005) 299–302, <https://doi.org/10.1557/JMR.2005.0048>.
- [27] R.L. Seibert, T.J. Gerczak, G.W. Helmreich, J.D. Hunn, AGR-2 irradiated TRISO particle IPyC/SiC interface analysis using FIB-SEM tomography, *J. Nucl. Mater.* 573 (2023), 154104, <https://doi.org/10.1016/j.jnucmat.2022.154104>.
- [28] C. Griesbach, T. Gerczak, Y. Zhang, P. Thevamaran, Microstructural heterogeneity of the buffer layer of TRISO nuclear fuel particles, *J. Nucl. Mater.* 574 (2022), 154219, <https://doi.org/10.1016/j.jnucmat.2022.154219>.
- [29] X. Zhao, R.M. Langford, I.P. Shapiro, P. Xiao, Onset plastic deformation and cracking behavior of silicon carbide under contact load at room temperature, *J. Am. Ceram. Soc.* 94 (2011) 3509–3514, <https://doi.org/10.1111/j.1551-2916.2011.04674.x>.
- [30] L. Zhao, J. Zhang, J. Pfitzing, M. Alam, A. Hartmaier, Depth-sensing ductile and brittle deformation in 3C-SiC under Berkovich nanoindentation, *Mater. Des.* 197 (2021), 109223, <https://doi.org/10.1016/j.matdes.2020.109223>.
- [31] H.P. Chen, R.K. Kalra, A. Nakano, P. Vashistha, I. Szlufarska, Multimillion-atom nanoindentation simulation of crystalline silicon carbide: Orientation dependence and anisotropic pileup, *J. Appl. Phys.* 102 (2007), <https://doi.org/10.1063/1.2781324>.
- [32] A.V. Samant, P. Pirouz, Activation parameters for dislocation glide in α -SiC, *Int. J. Refract. Met. Hard Mater.* 16 (1998) 277–289, [https://doi.org/10.1016/S0263-4368\(98\)00054-7](https://doi.org/10.1016/S0263-4368(98)00054-7).
- [33] C.A. Schuh, A.C. Lund, Application of nucleation theory to the rate dependence of incipient plasticity during nanoindentation, *J. Mater. Res.* 19 (2004) 2152–2158, <https://doi.org/10.1557/JMR.2004.0276>.
- [34] H. Wen, I.J. van Rooyen, Distribution of fission products palladium, silver, cerium and cesium in the un-corroded areas of the locally corroded SiC layer of a neutron irradiated TRISO fuel particle, *J. Eur. Ceram. Soc.* 37 (2017) 3271–3284, <https://doi.org/10.1016/j.jeurceramsoc.2017.04.012>.

- [35] D. Schappel, K.A. Terrani, Stress Profile in Coating Layers of TRISO Fuel Particles in Contact with One Another, *Nucl. Sci. Eng.* 196 (2022) 1349–1360, <https://doi.org/10.1080/00295639.2022.2090214>.
- [36] J.C. Bokros, Carbon biomedical devices, *Carbon N. Y.* 15 (1977) 353–371, [https://doi.org/10.1016/0008-6223\(77\)90324-4](https://doi.org/10.1016/0008-6223(77)90324-4).
- [37] D. Liu, K. Mingard, O.T. Lord, P. Flewitt, On the damage and fracture of nuclear graphite at multiple length-scales, *J. Nucl. Mater.* 493 (2017) 246–254, <https://doi.org/10.1016/j.jnucmat.2017.06.021>.
- [38] L. Payne, P.J. Heard, T.B. Scott, A study of the oxidation behaviour of pile grade A (PGA) nuclear graphite using thermogravimetric analysis (TGA), scanning electron microscopy (SEM) and x-ray tomography (XRT), *PLoS One* 10 (2015) 1–19, <https://doi.org/10.1371/journal.pone.0143041>.
- [39] A. Theodosiou, A.N. Jones, B.J. Marsden, Thermal oxidation of nuclear graphite: a large scale waste treatment option, *PLoS One* 12 (2017), e0182860, <https://doi.org/10.1371/journal.pone.0182860>.
- [40] A. Hodgkins, T.J. Marrow, M.R. Wootton, R. Moskvic, P.E.J. Flewitt, Fracture behaviour of radiolytically oxidised reactor core graphites: a view, *Energy Mater. Sci. Eng. Energy Syst.* 5 (2012) 899–907, <https://doi.org/10.1179/026708309X12526555493477>.